J Arid Land (2025) 17(12): 1785–1805
doi: 10.1007/s40333-025-0035-5; CSTR: 32276.14.JAL.02500355

Science Press Springer-Verlag

Comparison of different vegetation indices for estimating vegetation changes and analyzing driving factors in a semi-arid area, China

MA Yutao[1,2], GONG Jie[1,2*], JIN Tiantian[1,2], XU Tianyu[1,2], KAN Guobin[1,2]

[1] Key Laboratory of Western China's Environmental Systems (Ministry of Education), College of Earth and Environmental Sciences, Lanzhou University, Lanzhou 730000, China;
[2] Center for Remote Sensing of Ecological Environments in Cold and Arid Regions, Lanzhou University, Lanzhou 730000, China

Abstract: Climate warming and humidification trends have significantly influenced vegetation growth patterns in Chinese semi-arid areas. Exploring vegetation dynamics is crucial for understanding regional ecosystem structure and improving the efforts of ecosystem restoration. However, the applicability of various vegetation indices (VIs) in these arid areas remains uncertain. Evaluating the applicability of multiple VIs for vegetation monitoring can elucidate the variability of VIs performance at regional scale. Therefore, this study selected the Zuli River Basin (ZLRB), a typical loess hilly watershed in the semi-arid areas of China. Using Landsat data, we calculated the Normalized Difference Vegetation Index (NDVI), Enhanced Vegetation Index (EVI), and kernel NDVI (kNDVI) for the ZLRB from 1990 to 2020. We analyzed the spatiotemporal variations of these VIs using trend analysis and the Mann-Kendall test, and quantified the contributions of climate change (considering time-lag effects) and human activities to VIs changes through wavelet and residual analyses. Results indicated that VIs generally exhibited an upward trend in the ZLRB, with significant improvements observed in 54.91% of the area for NDVI, 31.69% for EVI, and 33.71% for kNDVI. Among them, NDVI outperformed EVI and kNDVI in capturing vegetation changes in the semi-arid area. VIs responded to precipitation with 1-month time lag and no time lag to temperature during growing season. Moreover, precipitation had a stronger positive correlation with VIs than temperature. Climate change was identified as the dominant driver of vegetation dynamics in the ZLRB, accounting for 93.12% of NDVI variation, while human activities contributed only 6.88%. Comparative analysis of VIs suggests that NDVI was more suitable for describing vegetation changes in the typical arid area of the ZLRB. Our findings underscore the importance of selecting appropriate VIs for targeted ecological restoration and sustainable land management.

Keywords: vegetation indices; spatiotemporal change; time-lag effect; climate change; human activities; the Zuli River Basin

Citation: MA Yutao, GONG Jie, JIN Tiantian, XU Tianyu, KAN Guobin. 2025. Comparison of different vegetation indices for estimating vegetation changes and analyzing driving factors in a semi-arid area, China. Journal of Arid Land, 17(12): 1785–1805. https://doi.org/10.1007/s40333-025-0035-5; https://cstr.cn/32276.14.JAL.02500355

1 Introduction

Vegetation, as a crucial component of terrestrial ecosystems, plays an indispensable role in the modeling of water, carbon, and energy cycles and exchanges (Liu et al., 2022b; Wang et al.,

*Corresponding author: GONG Jie (E-mail: jgong@lzu.edu.cn)
Received 2025-04-25; revised 2025-09-17; accepted 2025-10-09

2023b; Song et al., 2024). Its growth and phenology are strongly influenced by environmental changes, making monitoring vegetation essential for comprehending ecological processes and their response to climate-anthropogenic feedback mechanisms (Bai, 2021; Cheng et al., 2024). In addition, in arid and semi-arid areas, where water scarcity, desertification, and poor soil quality prevail, vegetation also contributes significantly to windbreak functions and reduction of soil erosion (Li et al., 2014). Consequently, scientifically monitoring vegetation changes is critical for comprehending regional ecosystem functioning and enhancing ecosystem restoration efforts (Fan et al., 2023).

Satellite-derived vegetation indices (VIs) such as Normalized Difference Vegetation Index (NDVI) and Enhanced Vegetation Index (EVI), are commonly used to quantify vegetation cover and dynamics. However, NDVI is susceptible to bare soil reflection with low vegetation cover and exhibits a nonlinear saturation relationship (Zhu et al., 2023a). To mitigate these limitations, EVI incorporates the blue band to improve saturation issues, yet it still lacks consideration of spatial heterogeneity. To make up for the above shortcomings, Camps-Valls et al. (2021) proposed the kernel NDVI (kNDVI), which leverages kernel functions to capture nonlinear relationships between spectral bands, and effectively solve the problem of mixed pixels (Camps-Valls et al., 2021). Since its development, many studies have used kNDVI in a range of research studies. For example, Zhang et al. (2024) introduced kNDVI and gross primary productivity to enhance regional ecological quality assessment. Ma et al. (2025) used the Standardized Precipitation Evapotranspiration Index (SPEI) and kNDVI to assess the drought resistance and resilience of natural and plantation forests in China. Zhao et al. (2023) demonstrated that replacing NDVI with kNDVI in constructing the kernel vegetation drought index improved capabilities for monitoring ecological drought conditions. Although NDVI, EVI, and kNDVI have been widely applied in environmental research, a systematic comparison of their responsiveness and applicability to environmental changes in semi-arid areas remains lacking. Therefore, a comprehensive evaluation of spatial applicability and temporal performance of these VIs is essential at the regional scale.

Currently, the interplay among vegetation cover, climate change, and human activities in semi-arid areas has become a prominent topic in global environmental research (Mo et al., 2019; Villani et al., 2024). Among these, climate change is widely recognized as the predominant driver of changes in vegetation cover within ecosystems (Higgins et al., 2023), particularly through its influence on temperature and precipitation patterns (Prăvălie et al., 2022). Although global climate warming can prolong the growing season and enhance carbon sequestration (Naeem et al., 2020), land-atmosphere feedbacks in drylands may offset these benefits and intensify drought stress (Yu et al., 2024). In addition, plants in semi-arid areas are heavily dependent on groundwater, which is primarily replenished by precipitation (Mo et al., 2019), making precipitation a critical determinant of plant physiological processes in such areas. However, the mechanisms by which temperature and precipitation affect vegetation is often nonlinear and exhibit hysteretic characteristics (Ma et al., 2023; Cheng et al., 2024). Studies have shown that earlier climatic conditions may have a more substantial impact on vegetation growth than current ones (Cheng et al., 2024). Incorporating time lag effects into climate-vegetation models has been shown to enhance their explanatory power by approximately 11.00% compared with models that ignore such lags (Wu et al., 2015). Therefore, considering time lag results is crucial for comprehensively capturing the feedback mechanism between vegetation and climate. In this context, comparing how different VIs respond to temperature and precipitation variations, particularly under lagged conditions, provides insights into their respective strengths in semi-arid climatic analyses.

Human interventions are widely recognized for their impacts on vegetation growth and phenology (Naeem et al., 2020). In response to ecosystem degradation, a series of large-scale ecological restoration projects have been implemented in China. Among these, the Grain for Green Project, as one of such ecological restorations, has significantly contributed to vegetation restoration (Cheng et al., 2024), playing a vital role in enhancing vegetation coverage and

aboveground biomass (Yang et al., 2022). However, some ecological projects that fail to adequately consider local environmental conditions may lead to unintended ecological and socio-economic consequences (Cao, 2011; Jia et al., 2017; Liu et al., 2022a; Wang et al., 2025a). For example, introducing water resources into arid areas can disrupt the competitive advantage of drought-tolerant plants, thereby affecting ecosystem carbon sequestration dynamics (Liu et al., 2022a). Similarly, the introduction of exotic tree species and high-density afforestation have led to a decrease in soil moisture of the Chinese Loess Plateau (Jia et al., 2017), and the Natural Forest Protection Program has resulted in an economic loss of 2.30×10^9 CNY in income for local herders in northern Shaanxi Province (Cao, 2011). Therefore, evaluating the performance of NDVI, EVI, and kNDVI in the context of human interventions is essential for quantifying vegetation-human feedbacks and for selecting the most appropriate indices for targeted vegetation monitoring.

The Zuli River Basin (ZLRB), located in the upper reaches of the Yellow River Basin (YRB), China, represents a typical semi-arid area characterized by fragile environment, low precipitation, and significant challenges in vegetation restoration (Liu et al., 2023b). Since the 1950s, numerous restoration initiatives have been undertaken to mitigate soil erosion and vegetation deterioration. These efforts have led to notable improvements in vegetation growth. Previous studies on vegetation status in arid areas of China, such as the Loess Plateau (Zheng et al., 2019a; Li et al., 2022b), have predominantly utilized NDVI data. However, relying solely on a single vegetation index may constrain the comprehensive understanding of vegetation responses to climatic and anthropogenic drivers. Although alternative indices like EVI and kNDVI have been developed, their applicability in semi-arid environments remains insufficiently investigated. In addition, while Moderate-resolution Imaging Spectroradiometer (MODIS) VIs has become widely used dataset in current vegetation research, their temporal resolution does not fully align with ecological restoration efforts since the 1990s. Additionally, their coarse spatial resolution limits the ability to capture fine-scale vegetation dynamics in small- and medium-sized catchments. Therefore, it is imperative to use Landsat series data to generate multiple VIs datasets suitable for the ZLRB. To address these research gaps, this study aims to: (1) generate NDVI, EVI, and kNDVI datasets during vegetation growing season from 1990 to 2020 using the Google Earth Engine platform and analyze spatial and temporal trends of these VIs across the ZLRB; (2) explore the time-lagged effects of climate change (precipitation and temperature) on VIs using partial correlation analysis and wavelet coherence methods; and (3) quantify the contributions of lagged climatic influences and human activities to vegetation dynamics using residual analysis.

2 Study area and data collection

2.1 Study area

The ZLRB, located in central Gansu Province and western part of Ningxia Hui Autonomous Region, China (35°17′–36°34′N, 104°12′–105°30′E), is a significant tributary of the YRB, covering an area of 1.06×10^4 km^2. The topography features higher elevation in the south and gradually descends towards lower elevation in the north, ranging from 1350 to 2776 m a.s.l. Notably, the basin has an arid climate with low precipitation, which exhibits a distinct latitudinal zonal distribution of precipitation, increasing progressively from north to south. The average annual precipitation is 388.92 mm, with 68.50% occurring during summer season (from June to September). In addition, the ZLRB showed an overall warming and wetting trend from 1990 to 2020, with annual average temperature rising by 0.28°C/10a and annual precipitation rising by 23.33 mm/10a. The ZLRB is characterized as a typical loess hill and gully area, which has long suffered from severe soil erosion and poor water quality, thus earning the nickname "Bitter Water River". Prior to 2000, annual average runoff was 1.10×10^8 m^3 and annual sediment load was 0.53×10^8 t, accounting for 1.06% and 39.60% of the total runoff and sediment transport into the YRB, respectively (Liu et al., 2023b). Therefore, there is a phenomenon of low water yield but

extremely high sediment yield, which intensifies severe soil and water loss. In combination with unfavorable climatic conditions that inhibit vegetation growth, this phenomenon poses a serious threat to regional ecology. However, over the past 60 a, a series of ecological restoration measures have been implemented in the ZLRB, including slope-to-terrace conversion (Tian et al., 2023), water conservancy project (Zhang et al., 2023), and the Grain for Green project (Zheng et al., 2019b). These integrated soil and water conservation measures have gradually developed into a comprehensive system, leading to a transition in the ecological environment from degradation to progressive restoration.

2.2 Data collection

2.2.1 Multi-vegetation index based on remote sensing

To ensure continuous and comprehensive temporal monitoring of vegetation dynamics, we used the Google Earth Engine platform to process the multi-temporal Landsat imagery of the ZLRB over the past 30 a. For this purpose, we selected three satellite images that include: (1) Landsat 5 Thematic Mapper (TM) surface reflectance datasets from 1990 to 2004 and from 2006 to 2011; (2) Landsat 7 TM surface reflectance datasets in 2005 and 2012; and (3) Landsat 8 Operational Land Imager/Thermal Infrared Sensor (OLI/TIRS) surface reflectance dataset from 2013 to 2020. All images underwent atmospheric and radiometric corrections using the Land Surface Reflectance Code (LaSRC) and Landsat Ecosystem Disturbance Adaptive Processing System (LEDAPS) algorithms.

The following pre-processing procedures were implemented to calculate the VIs with high quality and efficiency: (1) the Function of mask (F-mask) algorithm was used to identify and mask clouds and cloud shadows (Zhu et al., 2015), thereby enhancing the reliability of remote sensing data (Huete et al., 2002); (2) considering that vegetation growth rate in the YRB is significantly higher during summer (June, July, and August) compared with other seasons (Liu et al., 2023a), we selected June–August of each year (Prăvălie et al., 2022) as vegetation monitoring period for the ZLRB; (3) due to the Scan Line Corrector (SLC) failure of Landsat 7 ETM^+ scanner, there is a problem with missing bands in the images of 2012. To address this, we used TM5 images from 2011 to fill the missing areas in TM7 images from 2012; and (4) based on completed pre-processing and formulas of each VI using relevant spectral bands (such as blue band, red band, and near-infrared band), we constructed time series datasets of Landsat VIs.

2.2.2 Climate data collection and interpolation

We obtained the meteorological information of ZLRB by collecting data from 19 meteorological stations around the study area. These datasets were sourced from the China Meteorological Data Network (https://data.cma.cn/) and the Resource and Environmental Sciences Data Center of the Chinese Academy of Sciences (https://www.resdc.cn/). To ensure consistency with temporal and spatial resolution of VIs, we utilized ANUSPLIN v.4.4 software to generate monthly mean temperature and monthly cumulative precipitation with a spatial resolution of 30 m from 1990 to 2020. ANUSPLIN is a method that incorporates elevation data as a covariate to improve the accuracy of interpolation (Guo et al., 2020), making it particularly suitable for areas with significant topographical variations such as hilly and gully areas on the Loess Plateau. Furthermore, this software features robust parallel computing capabilities (Chen et al., 2024b), which significantly improve computational efficiency, making it well-suited for meteorological interpolation involving long time series.

2.2.3 Other data collection

Digital elevation data used in this study were obtained from the Shuttle Radar Topography Mission (SRTM), provided by the National Aeronautics and Space Administration (NASA) (http://earthexplorer.usgs.gov/), with a spatial resolution of 30 m, acquired in February 2000. These data served as a key covariate in the climate interpolation models. We gathered the ZLRB's land-use data with a spatial resolution of 30 m from the China's National Land Use and Cover Change (CNLUCC) that were provided by the Chinese Academy of Sciences Environmental and

Resource Science Data (https://www.resdc.cn/). The CNLUCC dataset classifies land use into six categories according to land resource characteristics and utilization attributes: farmland, woodland, grassland, water body, built-up land, and unused land.

3 Methods

3.1 Derivation of kNDVI

The kNDVI effectively alleviates the impact of mixed pixels and shows greater robustness to complex physical cyclic processes (Camps-Valls et al., 2021), thus providing a superior solution for mitigating saturation effects. The calculation of kNDVI is defined as follows:

$$\mathrm{kNDVI}=\frac{k(\rho_{\mathrm{NIR}},\rho_{\mathrm{NIR}})-k(\rho_{\mathrm{NIR}},\rho_R)}{k(\rho_{\mathrm{NIR}},\rho_{\mathrm{NIR}})+k(\rho_{\mathrm{NIR}},\rho_R)}, \tag{1}$$

where ρ_{NIR} and ρ_R are the reflectance in near-infrared and red channels, respectively; $k(\rho_{\mathrm{NIR}}, \rho_{\mathrm{NIR}})$ is the kernel function value of ρ_{NIR} and itself; and $k(\rho_{\mathrm{NIR}}, \rho_R)$ is the similarity measure between ρ_{NIR} and ρ_R under kernel function. Radial Basis Function (RBF) kernel is used, and its function is as follows:

$$k\left(\rho_{\mathrm{NIR}},\rho_R\right)=\mathrm{e}^{\frac{-(\rho_{\mathrm{NIR}}-\rho_R)^2}{2\sigma^2}}, \tag{2}$$

where σ is the length-scale parameter of the RBF, which controls the sensitivity of kernel to differences in reflectance; and e is the nature constant. This function captures higher-order relationships between spectral bands, reflecting its sensitivity to sparse and dense vegetation areas (Camps-Valls et al., 2021). The computational formulation can be simplified using a combination of kernel function and hyperbolic tangent function, as shown below:

$$\mathrm{kNDVI}=\frac{1-\mathrm{e}^{\left(-\frac{\left(\rho_{\mathrm{NIR}}-\rho_R\right)^2}{2\sigma^2}\right)}}{1+\mathrm{e}^{\left(-\frac{\left(\rho_{\mathrm{NIR}}-\rho_R\right)^2}{2\sigma^2}\right)}}=\tanh\left(\left(\frac{\rho_{\mathrm{NIR}}-\rho_R}{2\sigma}\right)^2\right), \tag{3}$$

where σ is set to 0.15 (dimensionless), following the configuration provided on the Google Earth Engine-based kNDVI platform (https://github.com/IPL-UV/kNDVI).

In this study, to comprehensively analyze the differences among various VIs for vegetation monitoring, in addition to kNDVI, we used the commonly applied NDVI and EVI. The calculations of NDVI and EVI are defined as follows:

$$\mathrm{NDVI}=\frac{\rho_{\mathrm{NIR}}-\rho_R}{\rho_{\mathrm{NIR}}+\rho_R}, \tag{4}$$

$$\mathrm{EVI}=\frac{G\times(\rho_{\mathrm{NIR}}-\rho_R)}{\rho_{\mathrm{NIR}}+C_1\times\rho_R-C_2\times\rho_B+L}, \tag{5}$$

where ρ_B is the reflectance in blue channel; G is the gain coefficient, and G=2.5; C_1 and C_2 are the coefficients of aerosol impedance term, respectively (C_1=6.0 and C_2=7.5); and L is the canopy background adjustment factor (L=1).

3.2 Vegetation trend analysis and variation test

Simple linear regression was applied to model the overall spatial variation pattern of vegetation at the pixel level. This method quantifies the linear trend of variables in area by calculating ordinary least squares estimates for each raster pixel (Liu et al., 2019). Its calculation is as follows:

$$\text{Slope} = \frac{n \times \sum_{i=1}^{n} (i \times \text{VI}_i) - \sum_{i=1}^{n} i \sum_{i=1}^{n} \text{VI}_i}{n \times \sum_{i=1}^{n} i^2 - \left(\sum_{i=1}^{n} i \right)^2}, \quad (6)$$

where Slope is the slope of trend line of multi-year linear regression equation for a single pixel (Li et al., 2022a; Tang et al., 2024), representing the inter-annual rate of change of VIs during growing season; i is the index of observation year (i=1, 2, …, 30); n is the span of years (n=30); and VI_i is the mean value of VIs during year i. Positive and negative values of Slope represent upward and downward trends in VIs, respectively.

To further elaborate on these trends, we classified them into five categories based on F-test significance (Table 1) (Liu et al., 2019).

Table 1 Quantitative categorization criteria for dynamic changes in vegetation indices (VIs) of the Zuli River Basin (ZLRB)

Classification	Categorization criterion
Significant increase	Slope>0, P<0.01
Insignificant increase	Slope>0, 0.01≤P<0.05
Insignificant increase	Slope>0, P≥0.05
Insignificant change	Slope=0
Insignificant decrease	Slope<0, P≥0.05
Insignificant decrease	Slope<0, 0.01≤P<0.05
Significant decrease	Slope<0, P<0.01

The Mann-Kendall test was employed to analyze the long-term trends of vegetation and climate change. As a nonparametric test, it is known for its robustness against outliers (Zuo et al., 2021). Its sample data do not need to adhere to a specific distribution and remain unaffected by a few exceptional values (Gong et al., 2022).

3.3 Calculation of time-lag effect of climate change

The process of vegetation growth is inherently gradual, and the response of VIs to climate change is not always synchronized (Liu et al., 2021). Furthermore, vegetation dynamics often exhibit a temporal lag in response to climate change (Ding et al., 2020). Therefore, this study took NDVI as an example and employed wavelet analysis to investigate the time-lag effects between vegetation and climate variables at the monthly scale. Wavelet analysis can capture the time and frequency domain characteristics of the sequence (Wang et al., 2024a). In climate and hydrology research, wavelet coherence analysis has become a key tool for exploring the interdependence between climate drivers and local drought responses (Bera et al., 2025). For example, recent studies have used wavelet analysis to investigate the interrelationships between climate indices and drought in various areas (Yeditha et al., 2023; Bera et al., 2025). The application of wavelet analysis has promoted drought prediction models (Hu et al., 2025) and improved early warning systems for climate adaptation (Yeditha et al., 2023). First, the continuous wavelet transform is used to reveal the local time-frequency characteristics of individual time series. Second, the resonance relationship between the two sequences at different time scales is analyzed by cross wavelet transform, and its correlation strength is quantified by combining wavelet coherence (Tomás et al., 2016; Chen et al., 2025). In addition, the lag time can be calculated by phase angle (Lian et al., 2022). Finally, the real part of cross wavelet transform is taken and normalized, that is, the wavelet cross-correlation is used to determine the mean time-lag relationship between NDVI and climate variables.

Partial correlation analysis is essential for distinguishing the independent effects of different climate indices on vegetation change, and can also be applied to explore interaction between analytical elements such as partial correlation network estimation (Wang et al., 2025b). The analysis is particularly effective in identifying the dominant factors of vegetation change, especially for drought-prone areas such as the Qilian Mountains (Liu et al., 2024a) and the arid areas in Central Asia (Wu et al., 2021). Using partial correlation analysis, combined with the results of wavelet analysis, we calculated the partial correlation between vegetation index and time-lagged climate change. Unlike Pearson's correlation analysis, this method allows the elimination of effect of other variables (Yang et al., 2022), thereby enabling a focused examination of individual variable impact on vegetation (Bai et al., 2024).

3.4 Impacts of climate change and human activities on vegetation dynamics

To quantify the impacts of climate change and human activities on vegetation changes in the ZLRB, we estimated the contribution of each driver to VIs on a pixel-by-pixel basis using a partial derivative approach (Zhang et al., 2016; Qu et al., 2020; Zhu et al., 2023b). Its calculation is as follows:

$$\frac{\mathrm{dVI}}{\mathrm{d}t} = \mathrm{TEM_{con}} + \mathrm{PRE_{con}} + \mathrm{HA_{con}} = \frac{\partial \mathrm{VI}}{\partial \mathrm{TEM}} \times \frac{\mathrm{dTEM}}{\mathrm{d}t} + \frac{\partial \mathrm{VI}}{\partial \mathrm{PRE}} \times \frac{\mathrm{dPRE}}{\mathrm{d}t} + \mathrm{HA_{con}}\ , \tag{7}$$

where dVI/dt is the annual rate of change of VIs in the time variable t; $\mathrm{TEM_{con}}$ and $\mathrm{PRE_{con}}$ are the contributions of temperature and precipitation to the inter-annual rate of change of VIs on a pixel-by-pixel basis, respectively; $\mathrm{HA_{con}}$ is the residual between inter-annual rate of change in VIs and the contribution of climate variables, which represents the contribution of other variables, such as anthropogenic factors dominated by fallowed land (Fan et al., 2023), carbon storage (Kolecka, 2021), and land use intensity (Shen et al., 2023) to the change rate in VIs; ∂VI/∂TEM and ∂VI/∂PRE are the partial derivatives of VIs with respect to temperature and precipitation, respectively; and dTEM/dt and dPRE/dt are the annual rates of change of temperature and precipitation calculated using the same method from Equation 6, respectively. Considering that each climate variable has a linear effect on the variation of VIs, the effect of other variables is eliminated by partial correlation analysis. Positive value of contribution indicates that the influencing factor contributes to the change of VIs and vice versa.

4 Results

4.1 Spatiotemporal changes and trend analysis of VIs

4.1.1 Spatiotemporal changes of VIs

From 1990 to 2020, the NDVI, EVI, and kNDVI exhibited an overall increasing trend, with linear growth rates of 0.0045/a, 0.0021/a, and 0.0035/a, respectively (Fig. 1). The observed ranges for NDVI, EVI, and kNDVI were 0.1760–0.4430, 0.1220–0.2610, and 0.0710–0.2830, respectively. According to the Mann-Kendall test results, most of the unformatted fit (UF) curves of these VIs were negative values from 1990 to 2000, indicating a degradation in VIs. Among the three indices, kNDVI exhibited a more pronounced negative UF trend before 2000, implying it may have responded more sensitively to early-stage vegetation degradation. Between 2000 and 2010, the UF curves showed smaller fluctuation, suggesting slower vegetation recovery in VIs. After 2010, UF values began to rise, and VIs crossed the 1.960 threshold around 2016, indicating statistically significant upward trends. Notably, from 2010 to 2020, NDVI demonstrated a significantly higher growth rate (0.0110/a) compared with EVI (0.0040/a) and kNDVI (0.0080/a), indicating that NDVI responded more rapidly to vegetation restoration. Compared with kNDVI, both NDVI and EVI displayed greater fluctuations between 2012 and 2014. After 2015, VIs improved markedly, possibly due to increased precipitation. In 2020, NDVI (0.4430), EVI (0.2600), and kNDVI (0.2830) reached their highest recorded values.

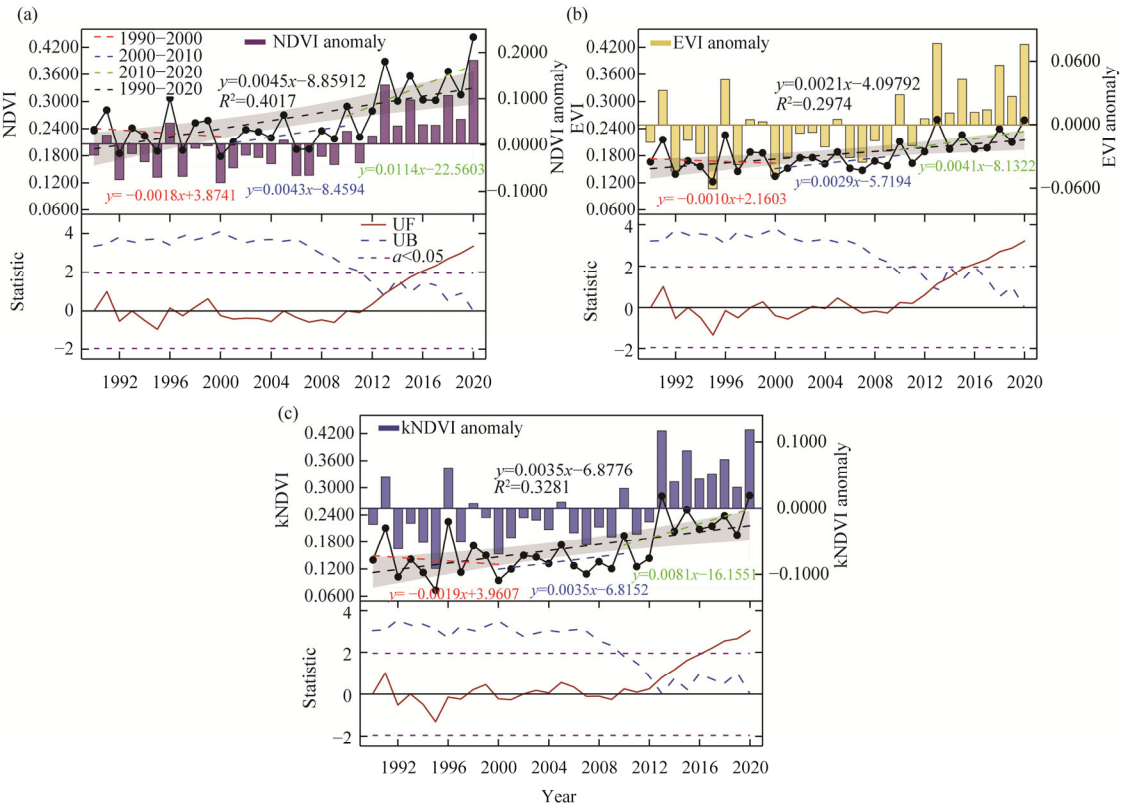

Fig. 1 Analysis of inter-annual variation, anomalies, and the Mann-Kendall trends of three different vegetation indices (VIs) in the Zuli River Basin (ZLRB) from 1990 to 2020. (a), NDVI (Normalized Difference Vegetation Index); (b), EVI (Enhanced Vegetation Index); (c), kernel NDVI (kNDVI). UF, unformatted fit; UB, underidentification bias. The shaded area indicates significance at the 95.00% confidence level.

4.1.2 Trend analysis

Based on quantitative evaluation in Table 1, we analyzed the trends of VIs in the ZLRB from 1990 to 2020 (Fig. 2). Overall, VIs consistently exhibited a trend of improvement across various areas. NDVI displayed a prominent increasing trend, with 54.91% significant increases of the total areas. Among different land use types, unused land demonstrated the highest rate of significant improvement, followed by woodland. The significant increase area for EVI accounted for 31.69% of the total area, primarily concentrated in the central ZLRB and southeastern Huining County. This proportion was smaller than those of NDVI and kNDVI. Similar to EVI, unused land again exhibited the highest rate of significant improvement, followed by woodland. Like EVI, the significant increase area in kNDVI reached 33.71%, with a similar spatial pattern, and woodland showed the highest improvement. In contrast, areas of significant decrease were small and scattered and mainly located in Jingyuan County, Anding District, and near the eastern and western tributary areas in the ZLRB, where built-up land experienced the most severe degradation, aligning with the overall spatial trends.

4.2 Contribution of climate drivers to inter-annual variation in VIs

4.2.1 Spatiotemporal variation trends of climatic variables

From 1990 to 2020, the average temperature exhibited an overall warming trend, with a linear growth rate of 0.28°C/10a (Fig. 3a and b). Results of the Mann-Kendall test indicated that temperature began to rise significantly following an abrupt change in 1997 and demonstrated a pronounced upward trend after 2000. Spatially, the temperature gradient decreased from northwest to southeast, while northern part of the ZLRB, located at lower elevations experienced

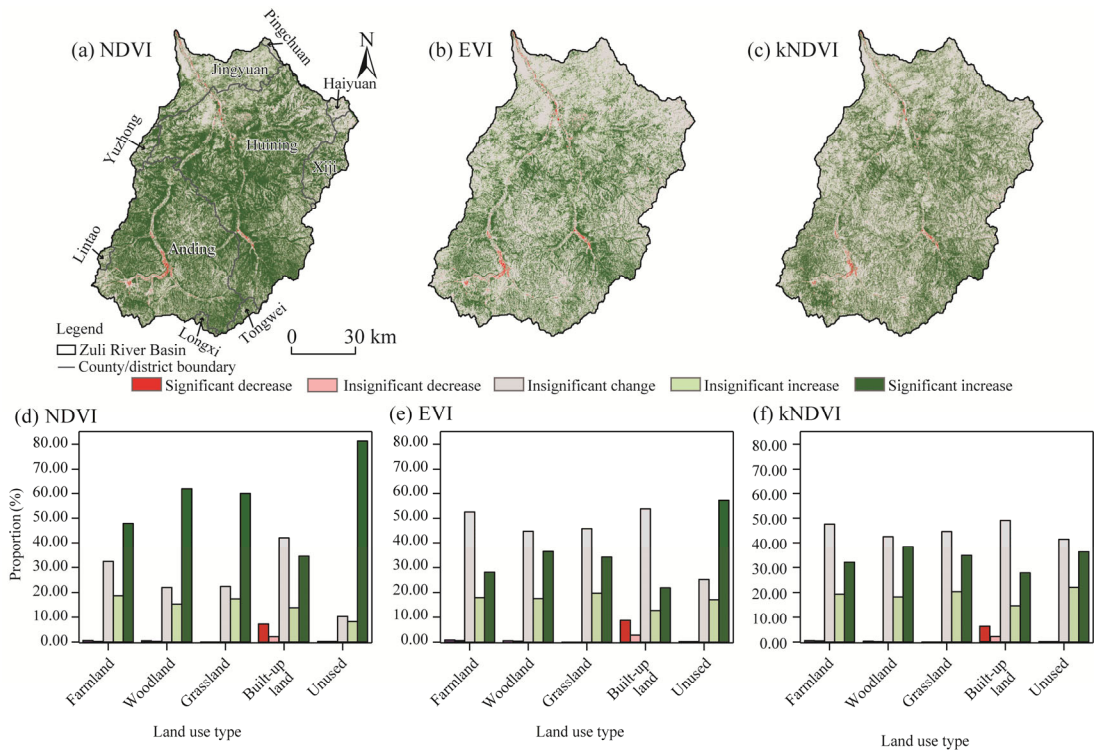

Fig. 2 Spatial change trends of VIs (a–c) and their proportions (d–f) to each land use type in the ZLRB from 1990 to 2020

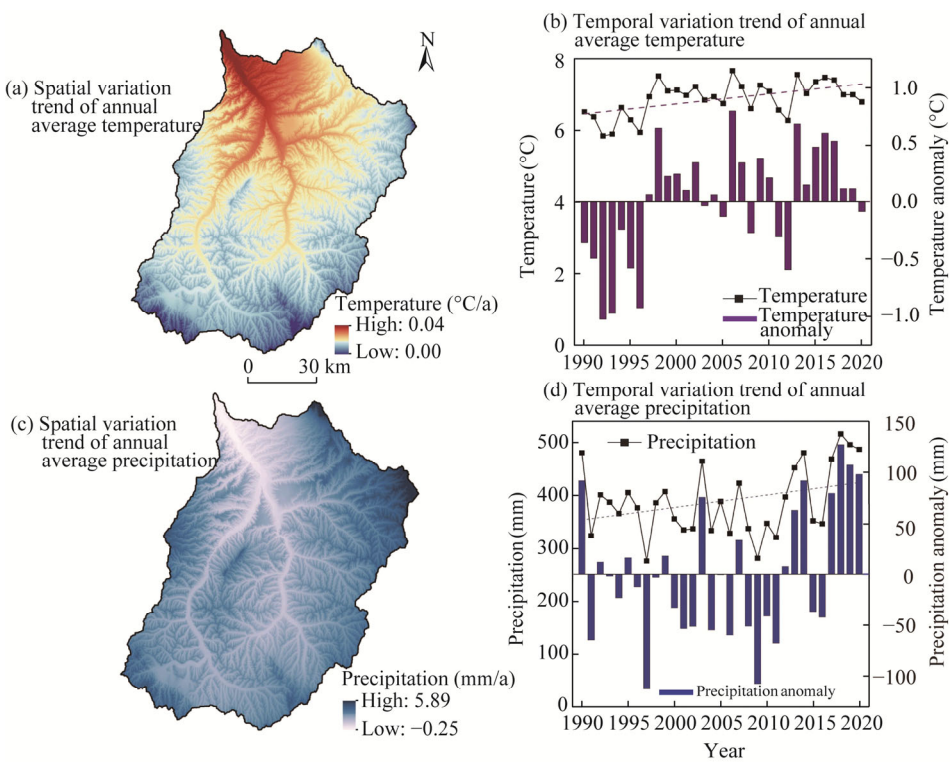

Fig. 3 Spatiotemporal variation trends of climatic variables in the ZLRB from 1990 to 2020. (a), spatial variation trend in annual average temperature; (b), temporal variation trend of annual average temperature; (c), spatial variation trend in annual average precipitation; (d), temporal variation trend of annual average precipitation.

a notable warming trend. Over the same period, annual average precipitation in the ZLRB also showed an overall increasing trend, with a linear growth rate of 23.33 mm/10a (Fig. 3c and d). However, the Mann-Kendall test results suggested that this increase was not statistically significant except for a marked shift observed in 2017. Spatially, average annual precipitation was influenced by elevation and exhibited a pattern of increasing from lower elevations towards surrounding areas, particularly with significant increases observed in northeastern part of the ZLRB.

4.2.2 Lag effects and partial correlation analysis between VIs and climate variables

Figure 4 shows the lag effect and the correlation between VIs and climate variables. To uniformly determine the lag months of VIs with climate variables, we selected NDVI as a representative of VIs to establish the lag relationship with climate change. From 1990 to 2020, NDVI, precipitation, and temperature exhibited consistent and significant periodicities of 8–16 months (Fig. 4a1–a3). Cross wavelet transform results showed that the resonance period of NDVI and climate variables during the study period was about 8–16 months (Fig. 4b1 and c1), but NDVI and climate variables did not vary perfectly synchronously. Specifically, NDVI exhibited a phase difference of about 7°–15° with temperature and about 35°–45° with precipitation in the wavelet coherence transform (Fig. 4b2 and c2), suggesting that there was a relative lag between these variables. Calculating the lag time based on phase angle yielded a lag of about 7–15 d for NDVI lagging

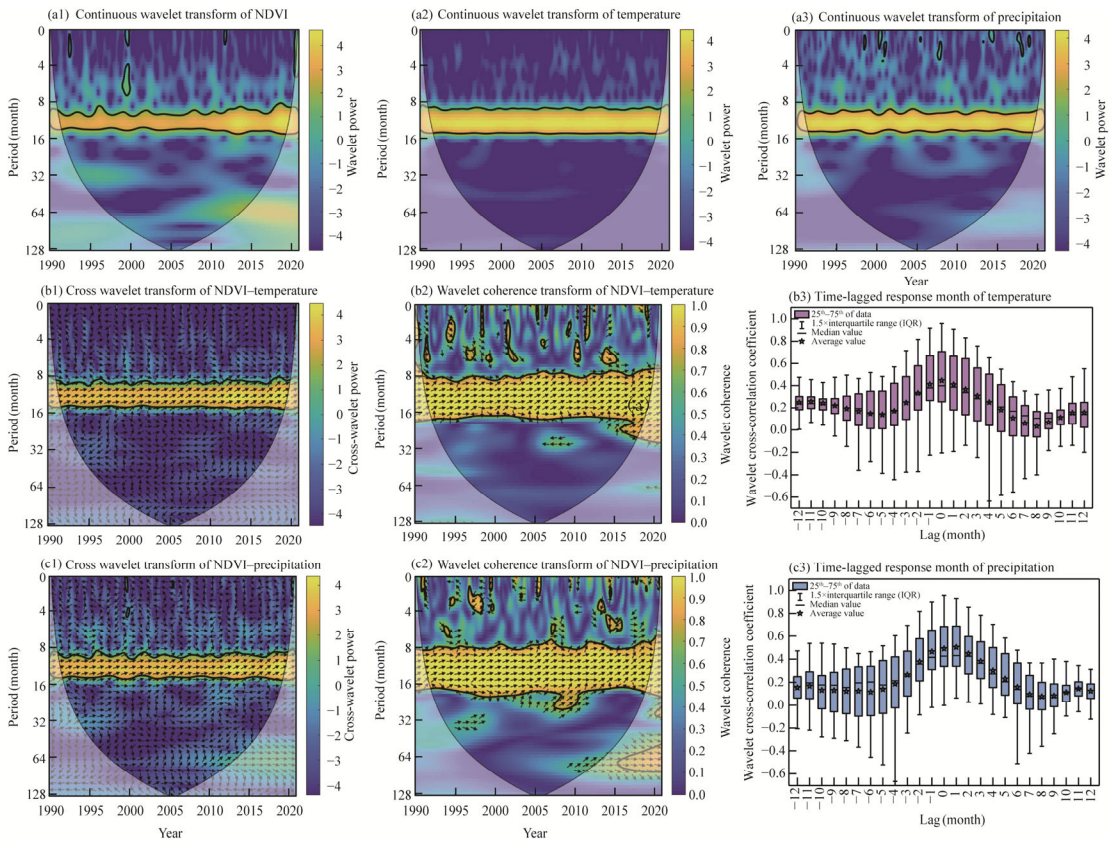

Fig. 4 Wavelet change analysis of monthly NDVI, precipitation, and temperature of the ZLRB from 1990 to 2020 and their corresponding lagged months. (a1–a3), wavelet power spectra of NDVI, precipitation, and temperature; (b1 and c1), cross wavelet transforms of NDVI–temperature and NDVI–precipitation; (b2 and c2), wavelet coherence transforms of NDVI–temperature and NDVI–precipitation; (b3 and c3), time-lagged response months of temperature and precipitation. The arrows in Figure b1, b2, c1, and c2 represent the relative phase relationship between two sequences. The negative lag values in Figure b3 and c3 indicate that NDVI leads climate variables, while the positive lag values indicate that NDVI lags behind climate variables.

temperature and about 35–45 d for precipitation. We plotted month-by-month box plots of NDVI versus climate variables from 1990 to 2020 based on wavelet cross-correlation coefficients (Fig. 4b3 and c3). Figure 4b3 showed the largest mean and median wavelet cross-correlation coefficients at 0-month time lag, indicating no lag between NDVI and temperature, which was similar to the wavelet coherence transform phase angle conclusion. Figure 4c3 had the largest average and median wavelet cross-correlation coefficients at 1 month, indicating a 1-month time lag of NDVI relative to precipitation.

Based on the results of wavelet analysis, we used precipitation with a 1-month time lag and temperature with 0-month time lag. To further investigate the spatial variations in lag effect, particularly among different VIs, we examined the spatial heterogeneity of this effect. The area showing a notable correlation between NDVI and temperature accounts for 14.68% of the total area, with an average partial correlation coefficient of 0.28, predominantly indicating positive correlations (Fig. 5a–c). Conversely, EVI exhibited fewer areas significantly correlated with temperature (11.25% of the total area) and had the lowest mean partial correlation coefficient (0.16). In addition, compared with NDVI, EVI demonstrated more areas with negative correlations, specifically concentrated within urban area across all three counties while appearing fragmented in eastern part of the ZLRB. The kNDVI displayed greater similarity to EVI. First, the percentage coverage of significant areas was 11.52%, and second, the biased correlation coefficient was similar (0.20). However, the difference lied in the higher distribution density observed within Huining County, which exhibited high positive bias correlations.

A total of 79.30% of the area exhibited significant correlations between NDVI and precipitation, with an average partial correlation coefficient of 0.49, predominantly indicating a positive correlation (Fig. 5d–f). High positive correlation areas were primarily concentrated in southeastern part of Huining County and northern part of Anding District. About 74.69% of the area showed positive correlations between EVI and precipitation. The spatial pattern was

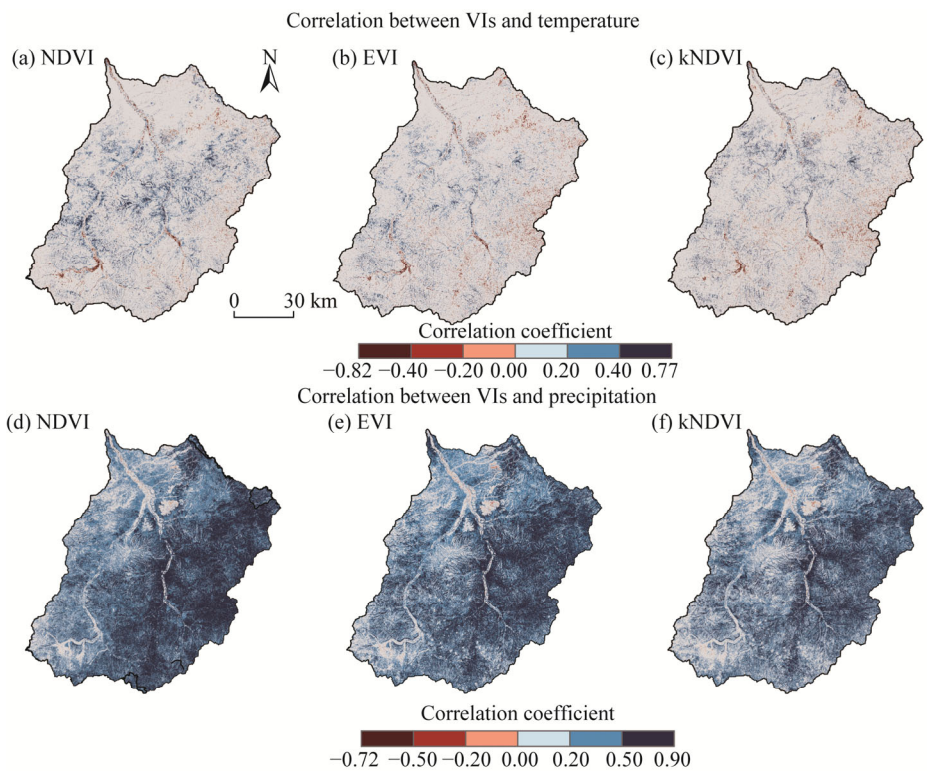

Fig. 5 Spatial distribution of partial correlation coefficients of VIs with temperature (a–c) and precipitation (d–f) of the ZLRB from 1990 to 2020

generally similar to that of NDVI but with weaker correlation strength. Among VIs, kNDVI exhibited the lowest proportion of positive correlation with precipitation (65.40%). Strong correlations (correlation coefficient>0.50) were primarily observed in eastern part of Huining County and parts of Haiyuan County, Xiji County, and surrounding areas.

4.2.3 Contribution of climatic variables to inter-annual variation of VIs

A partial derivative method was used to quantify the contribution of each factor to VIs from 1990 to 2020. The results revealed that climate variables exerted a positive influence on VIs (Fig. 6). Specifically, among the contributions of temperature to VIs, NDVI had the highest value (0.07%/a), followed by kNDVI (0.04%/a), and EVI (0.03%/a). Similarly, for the contributions of precipitation to VIs, NDVI ranked the highest (3.45%/a), followed by EVI (3.23%/a), and kNDVI (2.88%/a). Additionally, temperature and precipitation positively influenced NDVI, contributing 75.98% and 92.61% in the ZLRB, respectively.

Because of the longer growing season brought on by warmer temperature, which has greater beneficial effects on vegetation, temperature showed a positive effect, mainly in the central areas of the ZLRB. Consequently, positive contribution of temperature to NDVI surpassed that of EVI and kNDVI, making NDVI a more reliable indicator in this respect. In contrast, precipitation demonstrated a significant negative contribution, predominantly observed in northwestern part of the ZLRB, where lower elevation and abundant water resources reduce the reliance of vegetation on precipitation. Overall, when evaluating the spatial heterogeneity contributions of temperature and precipitation, NDVI outperformed EVI and kNDVI.

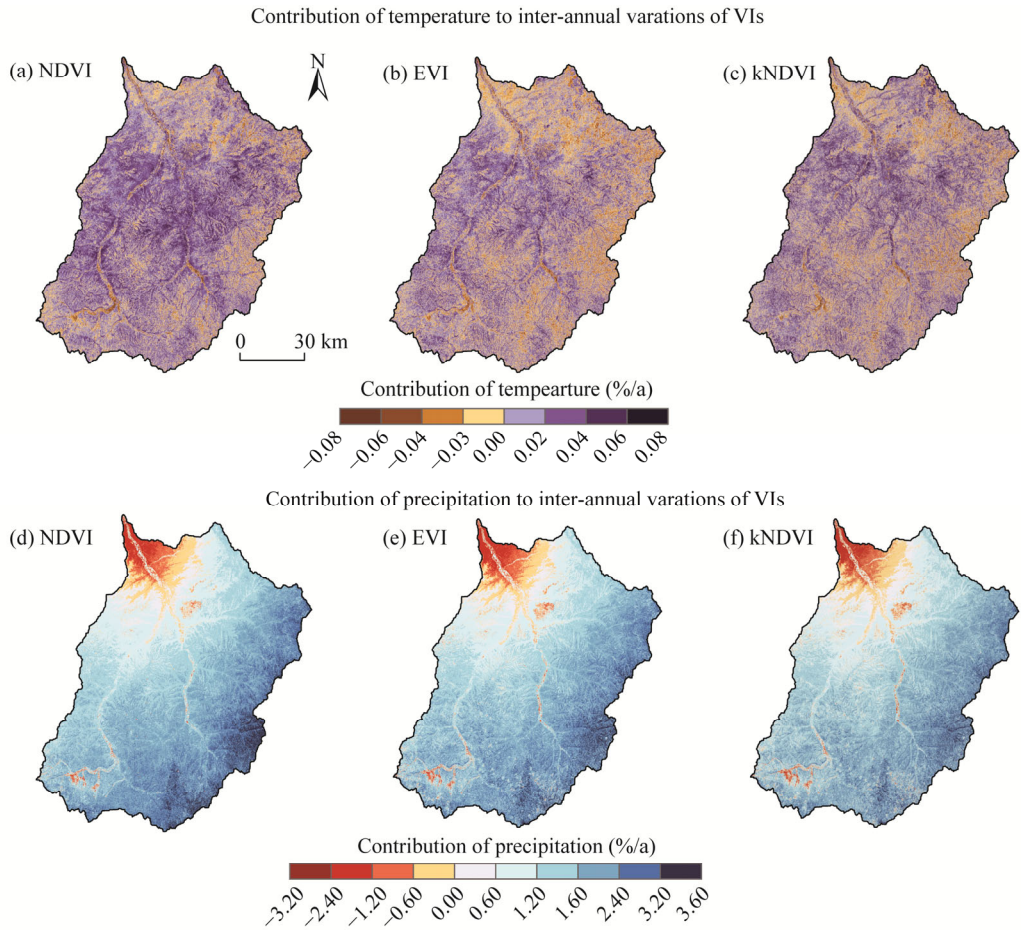

Fig. 6 Effects of climatic variables on inter-annual variations of VIs in the ZLRB. (a–c), contribution of temperature to inter-annual variation of VIs; (d–f), contribution of precipitation to inter-annual variation of VIs.

4.3 Contribution of climate change and human activities to changes in VIs

Quantifying the effects of climate change and human activities on vegetation cover can facilitate the implementation of local ecosystem management policies. Compared with human activities, climate variables were identified as the primary drivers behind the observed increase in vegetation greenness within the ZLRB (Fig. 7). When examining the climatic influences on VIs, it is evident that NDVI exhibited a larger positive contribution from climate change than EVI and kNDVI, particularly in southeastern area of the ZLRB. These areas predominantly consist of low- and medium-coverage grasslands, which are highly sensitive to the impact of climate change. From the perspective of land use, precipitation emerges as a significant contributor to the favorable impacts induced by climate change on land use types such as grassland, woodland, and unused land. Through analyzing human activities influencing VIs, it became apparent that human activities contributed more significantly (8.04%/a) to kNDVI than to NDVI (6.88%/a) and EVI (7.85%/a), primarily concentrated in rural residential areas and urban construction land in northwestern ZLRB. Woodland experienced various forms of anthropogenic disturbances, resulting in its greatest negative impact.

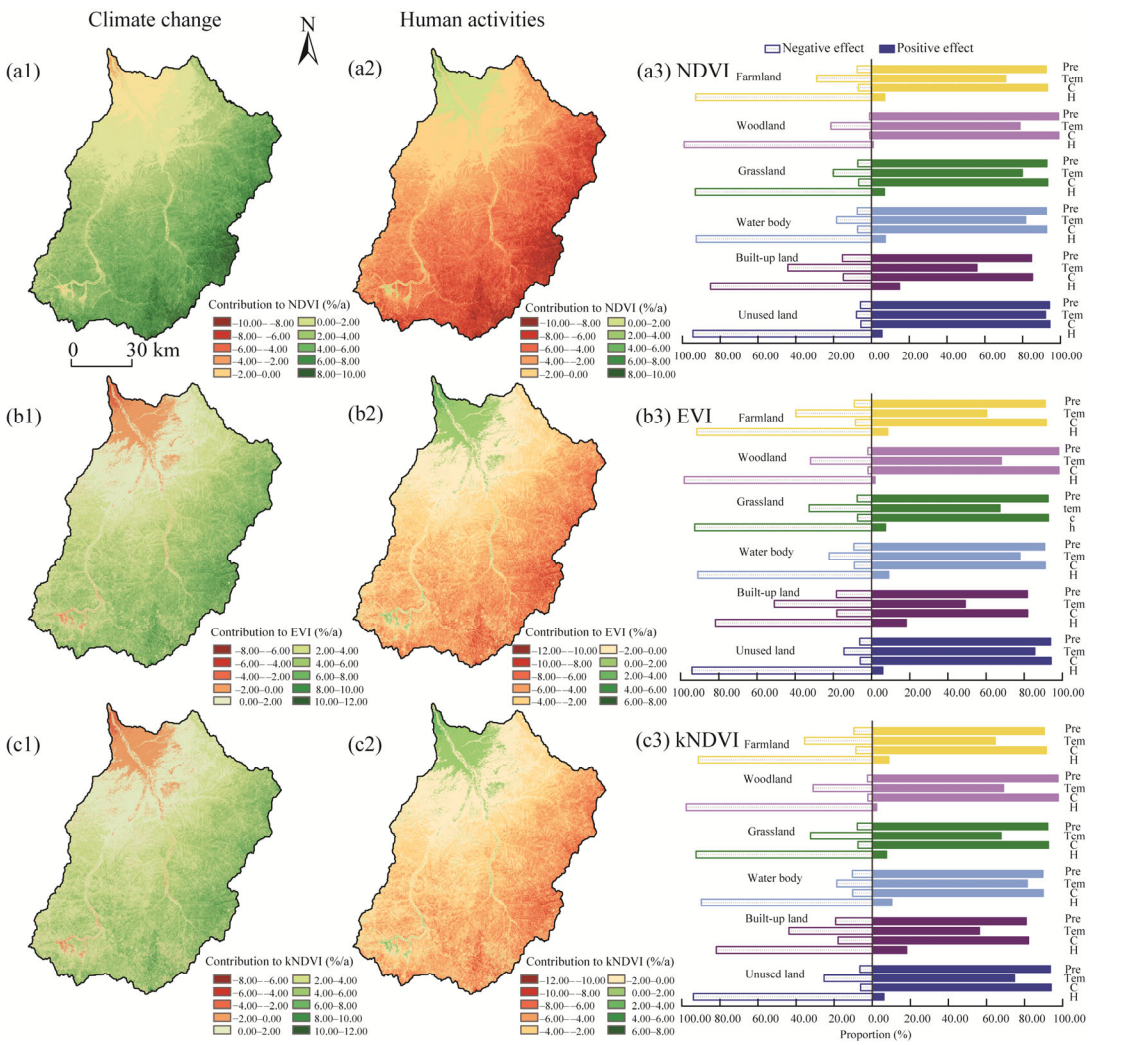

Fig. 7 Contributions of climate change (a1, b1, and c1) and human activities (a2, b2, and c2) to inter-annual variations of VIs and proportion of each land use type (a3, b3, and c3) affected by precipitation-lag (Pre), temperature-lag (Tem), climate change (C), and human activities (H) on VIs in the ZLRB

5 Discussion

5.1 Sentinel-2-based validation of Landsat-8 VIs

Compared with Landsat-8 images, Sentinel-2 images have two red edge bands. Benefiting from improved spatial and spectral resolution (10 m), Sentinel-2 provides more detailed spectral information, which facilitates the estimation of crop biophysical and biochemical indicators (Dong et al., 2020). Studies have found that Sentinel-2 images outperform Landsat-8 images in the accuracy and performance of estimating regional leaf area index (Sebastiani et al., 2023) and predicting regional vegetation aboveground biomass models (Xu et al., 2025). Some studies have also shown that the accuracy of Sentinel-2 images in predicting leaf area index is comparable to that of Landsat-8. Therefore, in remote sensing inversion of vegetation indices, comparing Landsat-8 VIs with those estimated from Sentinel-2 images can reveal the robustness of Landsat VIs dataset generated in this study. The vegetation growing season (June–August) in 2020 was selected as the study period. The three VIs showed high consistency between Sentinel-2 and Landsat-8 images, indicating that Landsat images can still effectively reflect regional vegetation conditions at medium spatial resolution.

In the two VIs datasets, the Sentinel-2 VIs values were smaller than the Landsat-8 VIs values. This difference may be due to variations in band design and sensor response mechanisms. Baldin and Casella (2025) found that the near-infrared band (842 nm) of Sentinel-2 Multispectral Imager and near-infrared band (865 nm) of Landsat-8 Operational Land Imager differed in spectral response characteristics. Sentinel-2 bands have narrower bandwidths and a spatial resolution of 20 m. Therefore, they showed higher sensitivity but yield lower index values in densely vegetated areas. As shown in Figure 8, VIs calculated from Sentinel-2 and Landsat-8 images showed a strong linear correlation at the sample points. The goodness of fit and Root Mean Square Error (RMSE) rankings were as follows: kNDVI (R^2=0.6837 and RMSE=0.105)>NDVI (R^2=0.6738 and RMSE=0.089)>EVI (R^2=0.6691 and RMSE=0.025). Among these, kNDVI had the highest goodness of fit, indicating that stronger robustness and cross-platform adaptability across different sensors. This result may be attributed to the kernel function form in kNDVI, which enhances the nonlinear difference expression between red and near-infrared bands (Wang et al., 2023a). EVI fitting performance was slightly inferior to NDVI, possibly due to the inclusion of blue band (Qiu et al., 2022) in its formula structure, which causes slight fluctuations in its performance across sensors. Overall, Landsat VIs showed consistent trends and strong correlations, which further verified the reliability of Landsat VIs produced in this study for spatial feature extraction and regional dynamic monitoring, thereby revealing the interactions among vegetation patterns, climate change, and human activities.

5.2 Impacts of climate change and human activities on VIs

Climate factors significantly influence vegetation development in terrestrial ecosystems (Wu et al., 2015). For instance, 92.61% of vegetation recovery in the ZLRB was attributed to precipitation. These findings are consistent with previous studies, highlighting precipitation as the primary driver of plant modifications in arid areas of China (Piao et al., 2014; Ma et al., 2022), particularly its significant correlation with lagged precipitation (Mo et al., 2019). Research indicates that global warming affects vegetation dynamics both in positive and negative ways (Allen et al., 2021; Dong et al., 2023a). Additionally, excessively high temperatures have been found to substantially increase the frequency of extreme weather events (Liu et al., 2024b), which subsequently affect plant community function (Chen et al., 2024c). In the ZLRB, vegetation responds most significantly to 1-month lagged precipitation and to temperature without lag (0-month time lag), as previously reported (Chen et al., 2025). Moreover, the impact of lagged precipitation far exceeds that of lagged temperature, which can be attributed to the unique topographic characteristics of the loess hilly area (Mo et al., 2019). Notably, annual precipitation

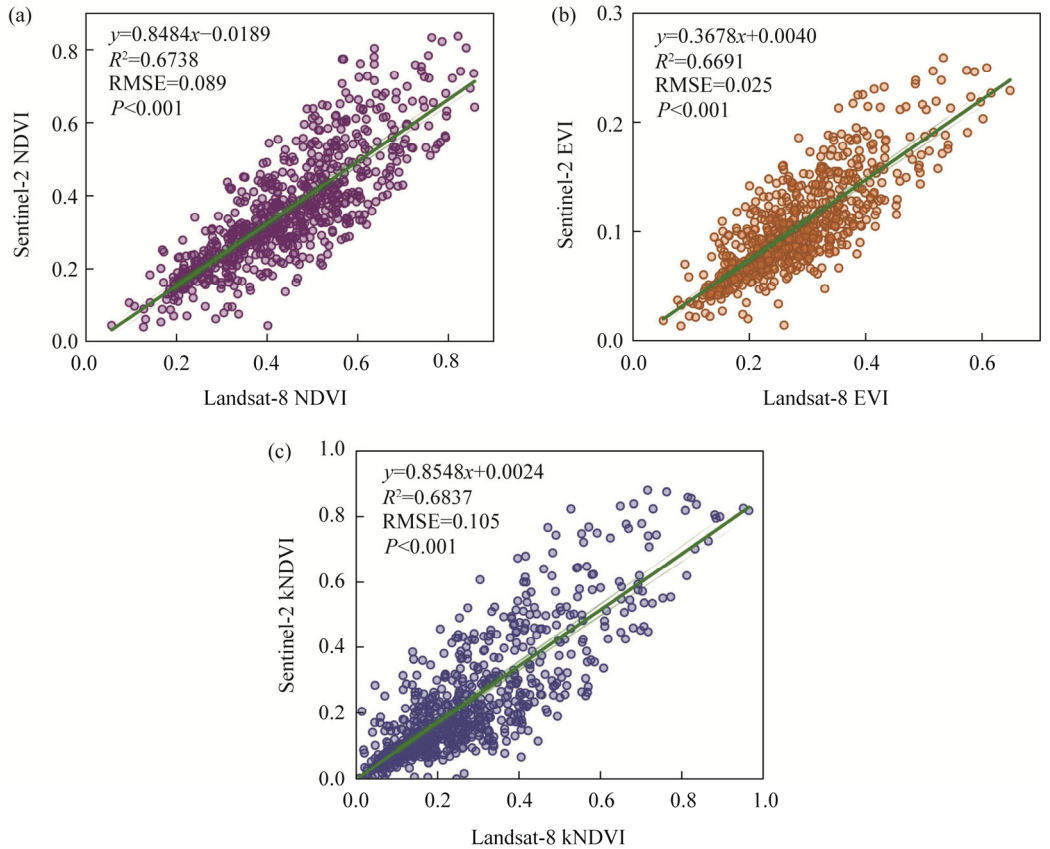

Fig. 8 Linear fitting relationships between Landsat-8 VIs and Sentinel-2 VIs. (a), NDVI; (b), EVI; (c), kNDVI. RMSE, Root Mean Square Error.

from 1990 to 2020 had a detrimental effect on downstream vegetation performance. Low annual precipitation, coupled with reduced vegetation cover and soil water infiltration in the downstream area of the ZLRB, may contribute to a decrease in soil organic matter, thereby inhibiting vegetation growth. Huang et al. (2023) reported that climate change and human activities contributed positively to vegetation change by 38.32% and 61.68%, respectively. Compared with studies that did not consider the hysteresis effect, our results showed that considering climate hysteresis could increase the contribution rate by up to 53.68%. Therefore, the hysteresis effect of precipitation in semi-arid areas has a dramatic impact on vegetation change.

Besides climate change, vegetation changes are significantly influenced by human activities (Shi et al., 2021). However, in this study, the impact of human activities on vegetation restoration was comparatively smaller than that of climate change. This finding may be closely related to regional ecological restoration projects. For example, several large-scale slope-to-terrace ecological management projects have been implemented in the ZLRB since the 1950s. Terracing have proven effective in enhancing soil water storage capacity (Huang et al., 2024), reducing runoff (Wang et al., 2024b), and providing flat farmland, all of which can positively influence vegetation cover (Chen et al., 2024a). The abandonment of terraces can potentially exert adverse effects on mountain vegetation communities (Rusterholz et al., 2020), carbon storage, and biodiversity (Dong et al., 2023b). Unlike many existing studies that broadly attribute vegetation improvement to large-scale ecological projects, our findings suggest a spatially differentiated and temporally constrained impact of human activities within the ZLRB. While ecological restoration initiatives have historically played a role in enhancing vegetation cover, our analysis reveals that actual positive contribution of human activities to vegetation dynamics was limited during the study period, particularly in the upstream and central areas. The study period coincided with an

intensification of terrace abandonment practices, which offsets the ecological benefits of earlier interventions. Human activities play a more prominent role in the lower reaches of the ZLRB, where they are positively influenced by ecological restoration programs such as the Grain for Green project (Zheng et al., 2019a) and the Three-North Shelterbelt program (Zhang et al., 2021). These spatial variations indicate that the effectiveness of human activities is neither uniform nor linear. It is necessary to assess its ecological impact in combination with topographic conditions, human resources, and socio-economic factors, so as to promote ecological restoration strategies tailored to local conditions. For example, research indicates that areas below an altitude of 1500 m with slopes less than 20° are more suitable for converting farmland into woodland (Qu et al., 2020). The downstream ZLRB features relatively gentle terrain and lower slopes, making it more conducive to the development of the Grain for Green project. However, in arid and semi-arid areas, ecological restoration projects may result in water consumption exceeding the carrying capacity of local water resources (Gong et al., 2022). Therefore, when planning future vegetation restoration initiatives in the ZLRB, it is advisable to explore coordinated utilization of abandoned terraces and to enhance farming subsidies for local farmers as effective strategies to facilitate vegetation restoration.

5.3 Applicability of NDVI, EVI, and kNDVI to semi-arid areas

Since the proposal of kNDVI by Camps-Valls et al. (2021), it has been applied in various ecological studies. Gu et al. (2024) used kNDVI to assess the response to multi-year droughts and to identify multi-year ecological drought events worldwide. Zhao et al. (2023) employed kNDVI to construct the kernel temperature vegetation drought index and demonstrated its applicability for ecological drought detection. However, in the context of fragile ecosystems in semi-arid areas of China, its advantages over traditional VIs such as NDVI and EVI remain to be further explored. Prior to this, some scholars also conducted comparative studies on multiple VIs. For example, Zhong and Li (2024) showed that the spatiotemporal variations of NDVI were more pronounced than those of EVI when analyzing urban vegetation greening. Henchiri et al. (2020) showed that NDVI was the most reliable predictor of soil productivity in arid areas when NDVI, EVI, and the soil adjusted VI were used to assess soil productivity. EVI exhibited greater inconsistency in predicting future vegetation trends in the Qinling-Daba Mountains (Bai, 2021).

A comparison of VIs across typical areas in the ZLRB (Fig. 9) revealed their respective strengths. Areas 1 and 4 in Figure 9, located at tributary confluences with low vegetation cover, were better represented by kNDVI in terms of growth status, whereas NDVI more accurately captured vegetation improvement. EVI tended to indicate degradation, aligning with Henchiri et al. (2020). Field surveys indicate that the ZLRB is largely arid with low species richness, making NDVI preferable in Areas 1 and 4 for reflecting vegetation improvement. Area 2, situated at higher elevation near Quwu Mountain, showed moderate vegetation cover. In this subarea, kNDVI and EVI performed better than NDVI in capturing vegetation changes influenced by topography. Notably, the mean values of NDVI and kNDVI differed significantly, highlighting the stability of EVI in balancing the two indices. Area 3, located in the area of Huajialing Town, had high vegetation cover. In terms of multi-year mean vegetation change, NDVI outperformed both EVI and kNDVI in this subarea, consistent with the findings of Zhong and Li (2024). In addition, kNDVI showed a tendency toward substantial biased here. Based on both the implementation timeline of slope terracing and field investigations, people conducted extensive slope terracing activities for crops cultivation purposes, such as maize farming. Consequently, highly skewed vegetation traits may arise, which prevent kNDVI from demonstrating superior performance compared with NDVI, consistent with Wang et al. (2023a). Overall, for studying the spatial pattern of vegetation change within the ZLRB, NDVI proved more suitable, whereas kNDVI and EVI were better suited for investigating how various factors impact vegetation response.

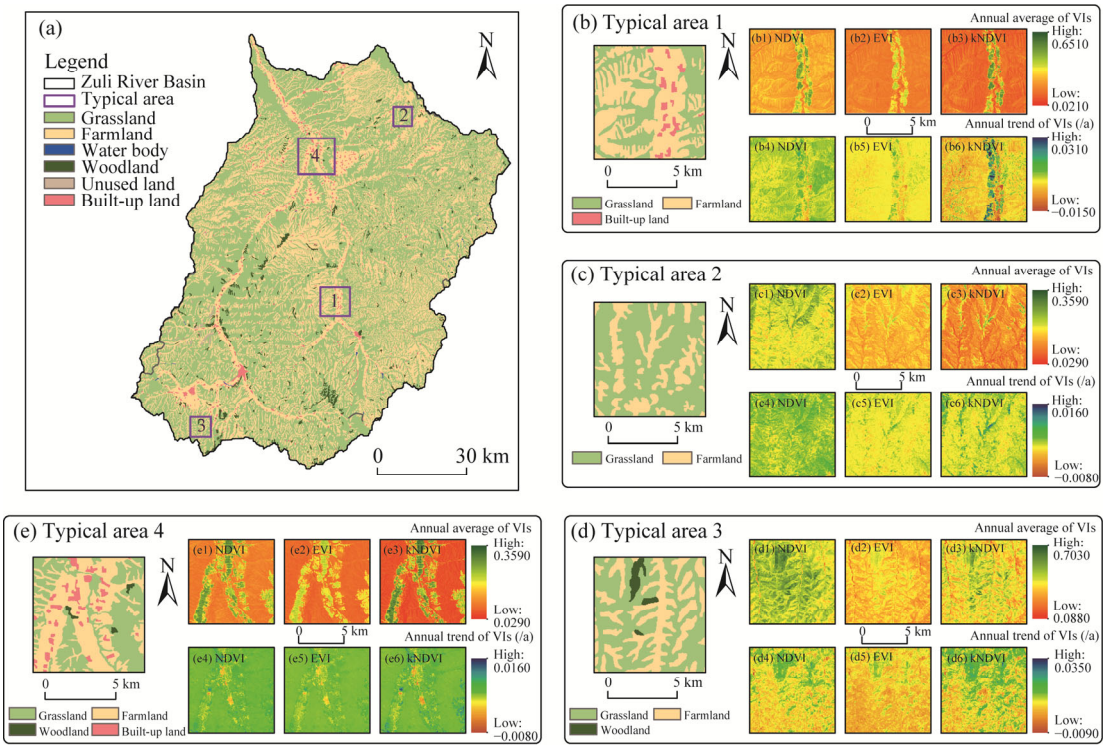

Fig. 9 Comparison of localized characteristics of typical areas of VIs in the ZLRB from 1990 to 2020. (a), typical area and land use type; (b1–b3, c1–c3, d1–d3, and e1–e3), annual average of VIs; (b4–b6, c4–c6, d4–d6, and e4–e6), annual trend of VIs.

5.4 Limitations and prospects

In this study, we aimed to identify the most appropriate vegetation index among NDVI, EVI, and kNDVI for characterizing vegetation phenology in typical arid areas of China. This research will assist in selecting suitable vegetation indices, particularly for studies focusing on arid areas. We examined the effects of climate change and human activities on VIs, while considering climate lag effects, thereby offering new perspectives for related fields. However, several limitations remain. First, the optimal selection of vegetation indices in arid areas considered only NDVI and EVI, overlooking other important indices such as the Ratio Vegetation Index, the Near-Infrared Reflectance of Vegetation, and the Difference Vegetation Index. Each index exhibits varying sensitivity to spectral response functions, and vegetation structure and composition, resulting in varying regional applicability (Fu et al., 2024). Second, this study focused solely on the hysteresis effects of temperature and precipitation, without considering potential cumulative effects. In light of increasing frequency of extreme climate events, future research should also explore how intense drought affects these phenomena. Lastly, since the ZLRB represents a typical area of slope conversion lands, incorporating spatial and temporal changes related to terraces in future studies is recommended. This approach could enable more accurate quantification of the contribution of human activities to vegetation change.

6 Conclusions

In this study, VIs such as NDVI, EVI, and kNDVI were constructed using the Landsat satellite series to study the spatiotemporal dynamics of vegetation in the ZLRB and their driving factors. By comparing VIs derived from Sentinel-2 and Landsat-8 images during the growing season in 2020, this study demonstrated the robustness and reliability of Landsat-derived VIs in characterizing vegetation patterns, thereby improving the accuracy of assessments regarding the

impacts of human activities and climate change on VIs. From 1990 to 2020, VIs showed similar fluctuations and upward trends. Notably, kNDVI performed better during periods of vegetation degradation, exhibiting the highest rate of decline. Temperature and precipitation exerted 0-month and 1-month time-lag effects on VIs, respectively. Climate change was the predominant influencing factor of vegetation change in the ZLRB relative to human activities, contributing 93.12% and 6.88% to the inter-annual variations of NDVI, respectively. Among them, NDVI was the most significant index to climate change, especially its sensitivity to temperature, and precipitation was higher than those of EVI and kNDVI. Furthermore, comparative analysis of VIs in typical areas of the ZLRB suggests that NDVI was more suitable for describing vegetation changes in the semi-arid areas. Based on these findings, future research should focus on monitoring ecological restoration processes using VIs, evaluating the effectiveness of various restoration strategies, and providing more precise guidance for sustainable land management and ecological conservation.

Conflict of interest

The authors declare that they have no known competing financial interests or personal relationships that could have appeared to influence the work reported in this paper.

Acknowledgements

This study was funded by the National Natural Science Foundation of China (U21A2011). Special thanks are due to the anonymous reviewers and the editors for their helpful comments that improved the manuscript substantially.

Author contributions

Conceptualization: MA Yutao, XU Tianyu; Methodology: JIN Tiantian; Formal analysis: MA Yutao, JIN Tiantian; Writing - original draft preparation: MA Yutao; Writing - review and editing: GONG Jie, JIN Tiantian, XU Tianyu; KAN Guobin; Funding acquisition: GONG Jie; Investigation: MA Yutao, KAN Guobin. All authors approved the manuscript.

References

Allen M A, Roberts D A, McFadden J P. 2021. Reduced urban green cover and daytime cooling capacity during the 2012–2016 California drought. Urban Climate, 36: 100768, doi: 10.1016/j.uclim.2020.100768.

Bai X L, Zhao W Z, Luo W C, et al. 2024. Effect of climate change on the seasonal variation in photosynthetic and non-photosynthetic vegetation coverage in desert areas, Northwest China. CATENA, 239: 107954, doi: 10.1016/j.catena.2024.107954.

Bai Y. 2021. Analysis of vegetation dynamics in the Qinling-Daba Mountains region from MODIS time series data. Ecological Indicators, 129: 108029, doi: 10.1016/j.ecolind.2021.108029.

Baldin C M, Casella V M. 2025. Comparison of planet scope and Sentinel-2 spectral channels and their alignment via linear regression for enhanced index derivation. Geosciences, 15(5): 184, doi: 10.3390/geosciences15050184.

Bera D, Dutta D, Poddar S, et al. 2025. Meteorological drought dynamics and climatic interactions in the arid and semi-arid regions of western India. Journal of Environmental Management, 387: 125836, doi: 10.1016/j.jenvman.2025.125836.

Camps-Valls G, Campos-Taberner M, Moreno-Martínez Á, et al. 2021. A unified vegetation index for quantifying the terrestrial biosphere. Science Advances, 7(9): eabc7447, doi: 10.1126/sciadv.abc7447.

Cao S X. 2011. Impact of China's large-scale ecological restoration program on the environment and society in arid and semiarid areas of China: Achievements, problems, synthesis, and applications. Critical Reviews in Environmental Science and Technology, 41(4): 317–335.

Chen D, Wei W, Chen L D, et al. 2024a. Response of soil nutrients to terracing and environmental factors in the Loess Plateau of China. Geography and Sustainability, 5(2): 230–240.

Chen L, Wei W, Tong B, et al. 2024b. Long-term terrace change and ecosystem service response in an inland mountain province of China. CATENA, 234: 107586, doi: 10.1016/j.catena.2023.107586.

Chen L L, Li Z H, Zhang C L, et al. 2025. Spatiotemporal changes of vegetation in the northern foothills of Qinling Mountains based on kNDVI considering climate time-lag effects and human activities. Environmental Research, 270: 120959, doi:

10.1016/j.envres.2025.120959.

Chen Y, Zhang T B, Zhu X, et al. 2024c. Quantitatively analyzing the driving factors of vegetation change in China: Climate change and human activities. Ecological Informatics, 82: 102667, doi: 10.1016/j.ecoinf.2024.102667.

Cheng M M, Wang Z H, Wang S D, et al. 2024. Determining the impacts of climate change and human activities on vegetation change on the Chinese Loess Plateau considering human-induced vegetation type change and time-lag effects of climate on vegetation growth. International Journal of Digital Earth, 17(1): 2336075, doi: 10.1080/17538947.2024.2336075.

Ding Y X, Li Z, Peng S Z. 2020. Global analysis of time-lag and -accumulation effects of climate on vegetation growth. International Journal of Applied Earth Observation and Geoinformation, 92: 102179, doi: 10.1016/j.jag.2020.102179.

Dong C Y, Yan Y, Guo J, et al. 2023a. Drought-vulnerable vegetation increases exposure of disadvantaged populations to heatwaves under global warming: A case study from Los Angeles. Sustainable Cities and Society, 93: 104488, doi: 10.1016/j.scs.2023.104488.

Dong S J, Xin L J, Li S F, et al. 2023b. Extent and spatial distribution of terrace abandonment in China. Journal of Geographical Sciences, 33(7): 1361–1376.

Dong T F, Liu J G, Qian B S, et al. 2020. Estimating crop biomass using leaf area index derived from Landsat 8 and Sentinel-2 data. ISPRS Journal of Photogrammetry and Remote Sensing, 168: 236–250.

Fan F F, Xiao C W, Feng Z M, et al. 2023. Impact of human and climate factors on vegetation changes in mainland Southeast Asia and Yunnan Province of China. Journal of Cleaner Production, 415: 137690, doi: 10.1016/j.jclepro.2023.137690.

Fu Y, Tan X P, Yao Y L, et al. 2024. Uncovering optimal vegetation indices for estimating wetland plant species diversity. Ecological Indicators, 166: 112367, doi: 10.1016/j.ecolind.2024.112367.

Gong X W, Li Y Q, Wang X Y, et al. 2022. Quantitative assessment of the contributions of climate change and human activities on vegetation degradation and restoration in typical ecologically fragile areas of China. Ecological Indicators, 144: 109536, doi: 10.1016/j.ecolind.2022.109536.

Gu Z P, Chen X W, Ruan W F, et al. 2024. Quantifying the direct and indirect effects of terrain, climate and human activity on the spatial pattern of kNDVI-based vegetation growth: A case study from the Minjiang River Basin, Southeast China. Ecological Informatics, 80: 102493, doi: 10.1016/j.ecoinf.2024.102493.

Guo B B, Zhang J, Meng X Y, et al. 2020. Long-term spatio-temporal precipitation variations in China with precipitation surface interpolated by ANUSPLIN. Scientific Reports, 10(1): 81, doi: 10.1038/s41598-019-57078-3.

Henchiri M, Liu Q, Essifi B, et al. 2020. Spatio-temporal patterns of drought and impact on vegetation in North and West Africa based on multi-satellite data. Remote Sensing, 12(23): 3869, doi: 10.3390/rs12233869.

Higgins S I, Conradi T, Muhoko E. 2023. Shifts in vegetation activity of terrestrial ecosystems attributable to climate trends. Nature Geoscience, 16(2): 147–153.

Hu M, Zhao X E, Chen F, et al. 2025. Increasing evidence of an anthropogenic signal in drought variations on the river source areas of southeastern Tibetan Plateau. Journal of Hydrology, 660: 133508, doi: 10.1016/j.jhydrol.2025.133508.

Huang C L, Xu J, Shan L X. 2023. Long-term variability of vegetation cover and its driving factors and effects over the Zuli River Basin in Northwest China. Sustainability, 15(3): 1829, doi: 10.3390/su15031829.

Huang Y, Wei W, Chen S N, et al. 2024. Effects of terracing with *Platycladus orientalis* plantations on water budget in the dryland of Loess Plateau in China. Ecological Engineering, 209: 107405, doi: 10.1016/j.ecoleng.2024.107405.

Huete A, Didan K, Miura T, et al. 2002. Overview of the radiometric and biophysical performance of the MODIS vegetation indices. Remote Sensing of Environment, 83(1–2): 195–213.

Jia X X, Shao M A, Zhu Y J, et al. 2017. Soil moisture decline due to afforestation across the Loess Plateau, China. Journal of Hydrology, 546: 113–122.

Kolecka N. 2021. Greening trends and their relationship with agricultural land abandonment across Poland. Remote Sensing of Environment, 257: 112340, doi: 10.1016/j.rse.2021.112340.

Li J, Wang J L, Zhang J, et al. 2022a. Growing-season vegetation coverage patterns and driving factors in the China-Myanmar Economic Corridor based on Google Earth Engine and geographic detector. Ecological Indicators, 136: 108620, doi: 10.1016/j.ecolind.2022.108620.

Li X R, Zhang Z S, Tan H J, et al. 2014. Ecological restoration and recovery in the wind-blown sand hazard areas of northern China: Relationship between soil water and carrying capacity for vegetation in the Tengger Desert. Science China Life Sciences, 57(5): 539–548.

Li X W, Zulkar H, Wang D Y, et al. 2022b. Changes in vegetation coverage and migration characteristics of center of gravity in the arid desert region of Northwest China in 30 recent years. Land, 11(10): 1688, doi: 10.3390/land11101688.

Lian X H, Jiao L M, Liu Z J, et al. 2022. Multi-spatiotemporal heterogeneous legacy effects of climate on terrestrial vegetation dynamics in China. GIScience & Remote Sensing, 59(1): 164–183.

Liu H X, Zhang A B, Liu C, et al. 2021. Analysis of the time-lag effects of climate factors on grassland productivity in Inner Mongolia. Global Ecology and Conservation, 30: e01751, doi: 10.1016/j.gecco.2021.e01751.

Liu J, Wei L H, Zheng Z P, et al. 2023a. Vegetation cover change and its response to climate extremes in the Yellow River Basin.

Science of the total Environment, 905: 167366, doi: 10.1016/j.scitotenv.2023.167366.

Liu L Y, Gou X H, Wang X J, et al. 2024a. Relationship between extreme climate and vegetation in arid and semi-arid mountains in China: A case study of the Qilian Mountains. Agricultural and Forest Meteorology, 348: 109938, doi: 10.1016/j.agrformet.2024.109938.

Liu M, Zhai H L, Zhang X C, et al. 2024b. Time-lag and accumulation responses of vegetation growth to average and extreme precipitation and temperature events in China between 2001 and 2020. Science of the Total Environment, 945: 174084, doi: 10.1016/j.scitotenv.2024.174084.

Liu Y, Liu H H, Chen Y, et al. 2022a. Quantifying the contributions of climate change and human activities to vegetation dynamic in China based on multiple indices. Science of the Total Environment, 838: 156553, doi: 10.1016/j.scitotenv.2022.156553.

Liu Y C, Li Z, Chen Y N, et al. 2022b. Evaluation of consistency among three NDVI products applied to High Mountain Asia in 2000–2015. Remote Sensing of Environment, 269: 112821, doi: 10.1016/j.rse.2021.112821.

Liu Y Y, Yang Y, Wang Q, et al. 2019. Evaluating the responses of net primary productivity and carbon use efficiency of global grassland to climate variability along an aridity gradient. Science of the Total Environment, 652: 671–682.

Liu Z M, Rong L, Wei W. 2023b. Impacts of land use/cover change on water balance by using the SWAT model in a typical loess hilly watershed of China. Geography and Sustainability, 4(1): 19–28.

Ma L L, Ma J, Yan P, et al. 2025. Planted forests in China have higher drought risk than natural forests. Global Change Biology, 31(2): e70055, doi: 10.1111/gcb.70055.

Ma M Y, Wang Q M, Liu R, et al. 2023. Effects of climate change and human activities on vegetation coverage change in northern China considering extreme climate and time-lag and -accumulation effects. Science of the Total Environment, 860: 160527, doi: 10.1016/j.scitotenv.2022.160527.

Ma Y R, Guan Q Y, Sun Y F, et al. 2022. Three-dimensional dynamic characteristics of vegetation and its response to climatic factors in the Qilian Mountains. CATENA, 208: 105694, doi: 10.1016/j.catena.2021.105694.

Mo K L, Chen Q W, Chen C, et al. 2019. Spatiotemporal variation of correlation between vegetation cover and precipitation in an arid mountain-oasis river basin in northwest China. Journal of Hydrology, 574: 138–147.

Naeem S, Zhang Y Q, Tian J, et al. 2020. Quantifying the impacts of anthropogenic activities and climate variations on vegetation productivity changes in China from 1985 to 2015. Remote Sensing, 12(7): 1113, doi: 10.3390/rs12071113.

Piao S L, Nan H J, Huntingford C, et al. 2014. Evidence for a weakening relationship between interannual temperature variability and northern vegetation activity. Nature Communications, 5(1): 5018, doi: 10.1038/ncomms6018.

Prăvălie R, Sîrodoev I, Nita I A, et al. 2022. NDVI-based ecological dynamics of forest vegetation and its relationship to climate change in Romania during 1987–2018. Ecological Indicators, 136: 108629, doi: 10.1016/j.ecolind.2022.108629.

Qiu R N, Li X, Han G, et al. 2022. Monitoring drought impacts on crop productivity of the U.S. Midwest with solar-induced fluorescence: GOSIF outperforms GOME-2 SIF and MODIS NDVI, EVI, and NIRv. Agricultural and Forest Meteorology, 323: 109038, doi: 10.1016/j.agrformet.2022.109038.

Qu S, Wang L C, Lin A W, et al. 2020. Distinguishing the impacts of climate change and anthropogenic factors on vegetation dynamics in the Yangtze River Basin, China. Ecological Indicators, 108: 105724, doi: 10.1016/j.ecolind.2019.105724.

Rusterholz H P, Binggeli D, Baur B. 2020. Successful restoration of abandoned terraced vineyards and grasslands in Southern Switzerland. Basic and Applied Ecology, 42: 35–46.

Sebastiani A, Salvati R, Manes F. 2023. Comparing leaf area index estimates in a Mediterranean forest using field measurements, Landsat 8, and Sentinel-2 data. Ecological Processes, 12(1): 28, doi: 10.1186/s13717-023-00441-0.

Shen F X, Yang L, Zhang L, et al. 2023. Quantifying the direct effects of long-term dynamic land use intensity on vegetation change and its interacted effects with economic development and climate change in Jiangsu, China. Journal of Environmental Management, 325: 116562, doi: 10.1016/j.jenvman.2022.116562.

Shi S Y, Yu J J, Wang F, et al. 2021. Quantitative contributions of climate change and human activities to vegetation changes over multiple time scales on the Loess Plateau. Science of the Total Environment, 755: 142419, doi: 10.1016/j.scitotenv.2020.142419.

Song X Y, Xie P J, Sun W Y, et al. 2024. The greening of vegetation on the Loess Plateau has resulted in a northward shift of the vegetation greenness line. Global and Planetary Change, 237: 104440, doi: 10.1016/j.gloplacha.2024.104440.

Tang J J, Liu D D, Shang C J, et al. 2024. Impacts of land use change on surface infiltration capacity and urban flood risk in a representative karst mountain city over the last two decades. Journal of Cleaner Production, 454: 142196, doi: 10.1016/j.jclepro.2024.142196.

Tian P, Tian X J, Geng R, et al. 2023. Response of soil erosion to vegetation restoration and terracing on the Loess Plateau. CATENA, 227: 107103, doi: 10.1016/j.catena.2023.107103.

Tomás R, Li Z, Lopez-Sanchez J M, et al. 2016. Using wavelet tools to analyse seasonal variations from InSAR time-series data: A case study of the Huangtupo landslide. Landslides, 13(3): 437–450.

Villani L, Castelli G, Yimer E A, et al. 2024. Impacts of climate change and vegetation response on future aridity in a

Mediterranean catchment. Agricultural Water Management, 299: 108878, doi: 10.1016/j.agwat.2024.108878.
Wang Q, Moreno-Martínez Á, Muñoz-Marí J, et al. 2023a. Estimation of vegetation traits with kernel NDVI. ISPRS Journal of Photogrammetry and Remote Sensing, 195: 408–417.
Wang S J, Chen F, Chen Y P, et al. 2025a. Greening of Eurasia's center driven by low-latitude climate warming. Forest Ecosystems, 13: 100330, doi: 10.1016/j.fecs.2025.100330.
Wang S N, Zhou Q C, Wu Y J, et al. 2024a. Drought lag and its cumulative effects on vegetation dynamics and response to atmospheric circulation factors in Yinshanbeilu, Inner Mongolia. Global Ecology and Conservation, 54: e03087, doi: 10.1016/j.gecco.2024.e03087.
Wang Y H, Yang A X, Shen W H, et al. 2024b. Spatial patterns, determinants, future trends, and implications for the sustainable use of terraces abandonment in China. Journal of Cleaner Production, 467: 142860, doi: 10.1016/j.jclepro.2024.142860.
Wang Z, Wang Y C, Liu Y, et al. 2023b. Spatiotemporal characteristics and natural forces of grassland NDVI changes in Qilian Mountains from a sub-basin perspective. Ecological Indicators, 157: 111186, doi: 10.1016/j.ecolind.2023.111186.
Wang Z Z, Fu B J, Wu X T, et al. 2025b. Exploring the interdependencies of ecosystem services and social-ecological factors on the Loess Plateau through network analysis. Science of the Total Environment, 960: 178362, doi: 10.1016/j.scitotenv.2024.178362.
Wu D H, Zhao X, Liang S L, et al. 2015. Time-lag effects of global vegetation responses to climate change. Global Change Biology, 21(9): 3520–3531.
Wu L Z, Ma X F, Dou X, et al. 2021. Impacts of climate change on vegetation phenology and net primary productivity in arid Central Asia. Science of the Total Environment, 796: 149055, doi: 10.1016/j.scitotenv.2021.149055.
Xu Y M, Qin Y M, Li B, et al. 2025. Estimating vegetation aboveground biomass in Yellow River Delta coastal wetlands using Sentinel-1, Sentinel-2 and Landsat-8 imagery. Ecological Informatics, 87: 103096, doi: 10.1016/j.ecoinf.2025.103096.
Yang S K, Liu J, Wang C H, et al. 2022. Vegetation dynamics influenced by climate change and human activities in the Hanjiang River Basin, Central China. Ecological Indicators, 145: 109586, doi: 10.1016/j.ecolind.2022.109586.
Yeditha P K, Anusha G S, Nandikanti S S S, et al. 2023. Development of monthly scale precipitation-forecasting model for Indian Subcontinent using wavelet-based deep learning approach. Water, 15(18): 3244, doi: 10.3390/w15183244.
Yu X J, Zhang L X, Zhou T J, et al. 2024. Higher atmospheric aridity-dominated drought stress contributes to aggravating dryland productivity loss under global warming. Weather and Climate Extremes, 44: 100692, doi: 10.1016/j.wace.2024.100692.
Zhang D N, Zuo X X, Zang C F. 2021. Assessment of future potential carbon sequestration and water consumption in the construction area of the Three-North Shelterbelt Programme in China. Agricultural and Forest Meteorology, 303: 108377, doi: 10.1016/j.agrformet.2021.108377.
Zhang X Y, Jia W W, Lu S X, et al. 2024. Ecological assessment and driver analysis of high vegetation cover areas based on new remote sensing index. Ecological Informatics, 82: 102786, doi: 10.1016/j.ecoinf.2024.102786.
Zhang Y, Zhang C B, Wang Z Q, et al. 2016. Vegetation dynamics and its driving forces from climate change and human activities in the Three-River Source Region, China from 1982 to 2012. Science of the Total Environment, 563–564: 210–220.
Zhang Z H, Zhang F, Zhang Z Z, et al. 2023. Study on water quality change trend and its influencing factors from 2001 to 2021 in Zuli River Basin in the northwestern part of the Loess Plateau, China. Sustainability, 15(8): 6360, doi: 10.3390/su15086360.
Zhao J P, Guo E H, Wang Y F, et al. 2023. Ecological drought monitoring of Inner Mongolia vegetation growing season based on kernel temperature vegetation drought index (kTVDI). Chinese Journal of Applied Ecology, 34(11): 2929–2937. (in Chinese)
Zheng K, Wei J Z, Pei J Y, et al. 2019a. Impacts of climate change and human activities on grassland vegetation variation in the Chinese Loess Plateau. Science of the Total Environment, 660: 236–244.
Zheng K, Ye J S, Jin B C, et al. 2019b. Effects of agriculture, climate, and policy on NDVI change in a semi-arid river basin of the Chinese Loess Plateau. Arid Land Research and Management, 33(3): 321–338.
Zhong Q K, Li Z. 2024. Long-term trends of vegetation greenness under different urban development intensities in 889 global cities. Sustainable Cities and Society, 106: 105406, doi: 10.1016/j.scs.2024.105406.
Zhu C C, Tian J, Tian Q J, et al. 2023a. Using NDVI-NSSI feature space for simultaneous estimation of fractional cover of non-photosynthetic vegetation and photosynthetic vegetation. International Journal of Applied Earth Observation and Geoinformation, 118: 103282, doi: 10.1016/j.jag.2023.103282.
Zhu L Y, Sun S, Li Y, et al. 2023b. Effects of climate change and anthropogenic activity on the vegetation greening in the Liaohe River Basin of northeastern China. Ecological Indicators, 148: 110105, doi: 10.1016/j.ecolind.2023.110105.
Zhu Z, Wang S X, Woodcock C E. 2015. Improvement and expansion of the Fmask algorithm: Cloud, cloud shadow, and snow detection for Landsats 4–7, 8, and Sentinel 2 images. Remote Sensing of Environment, 159: 269–277.
Zuo D P, Han Y, Xu Z X, et al. 2021. Time-lag effects of climatic change and drought on vegetation dynamics in an alpine river basin of the Tibet Plateau, China. Journal of Hydrology, 600: 126532, doi: 10.1016/j.jhydrol.2021.126532.